Published in final edited form as:
Biofabrication. 2013 June ; 5(2): 025004. doi:10.1088/1758-5082/5/2/025004.

Characterization of Printable Cellular Micro-fluidic Channels for Tissue Engineering

Yahui Zhang[1,3], **Yin Yu**[2,3], **Howard Chen**[1,3], and **Ibrahim T. Ozbolat**[1,3]

Ibrahim T. Ozbolat: ibrahim-ozbolat@uiowa.edu

[1]Mechanical and Industrial Engineering Department, The University of Iowa, Iowa City, IA, USA

[2]Biomedical Engineering Department, The University of Iowa, Iowa City, IA, USA

[3]Biomanufacturing Laboratory, Center for Computer-Aided Design, The University of Iowa, Iowa City, IA, USA

Abstract

Tissue engineering has been a promising field of research, offering hope of bridging the gap between organ shortage and transplantation needs. However, building three-dimensional (3D) vascularized organs remains the main technological barrier to be overcome. One of the major challenges is the inclusion of a vascular network to support cell viability in terms of nutrients and oxygen perfusion. This paper introduces a new approach to fabrication of vessel-like microfluidic channels that has the potential to be used in thick tissue or organ fabrication in the future. In this research, we investigate the manufacturability of printable micro-fluidic channels, where micro-fluidic channels support mechanical integrity as well as enable fluid transport in 3D. A pressure-assisted solid freeform fabrication platform is developed with a coaxial needle dispenser unit to print hollow hydrogel filaments. The dispensing rheology is studied, and effects of material properties on structural formation of hollow filaments are analyzed. Sample structures are printed through the developed computer-controlled system. In addition, cell viability and gene expression studies are presented in this paper. Cell viability shows that cartilage progenitor cells (CPCs) maintained their viability right after bioprinting and during prolonged *in vitro* culture. Real-time PCR analysis yielded relatively higher expression of cartilage-specific genes in alginate hollow filament encapsulating CPCs, compared with monolayer cultured CPCs, which revealed that printable semi-permeable micro-fluidic channels provided an ideal environment for cell growth and function.

1. Introduction

Despite the progress in tissue engineering, manufacturing and integration of vascular networks is still a challenge in thick tissue and organ fabrication. Without vascularization, three-dimensional (3D) engineered thick tissues or organs cannot get enough nutrients, gas exchange, and waste removal, all of which are needed for maturation during perfusion [1]. Systems must be developed to transport nutrients, growth factors, and oxygen to cells while extracting metabolic waste products such as lactic acid, carbon dioxide, and hydrogen ions so the cells can grow and fuse together, forming large-scale tissues and organs. Cells in a 3D organ structure cannot maintain their metabolic functions without this ability, which is traditionally provided by blood vessels. Biomanufacturing technology, on the other hand,

currently does not allow multi-scale tissue fabrication where bifurcated vessels are required to be manufactured with capillaries to mimic natural vascular anatomy [2]. Although several researchers have investigated developing vascular trees using computer models, generating massive amount of digital data [3], only a few attempts have been made toward fabricating bifurcated or branched channels so far with a representative model fabricated using tissue spheroids [4]. Successful maturation towards functional mechanically integrated bifurcated vessels is still a challenge.

As an alternative to biomimetically fabricated bifurcated vessels, one possible solution to improve perfusion through thick tissues is embedded micro-fluidic networks. Lee *et al.* [5] showed the great difference in cell viability between scaffolds with and without micro-fluidic channels. Ling *et al.* [6] demonstrated that micro-fluidic channels can efficiently deliver nutrients to encapsulated cells and showed a higher cell viability when the cells were closer to the micro-fluidic channel. Micro-fluidic channel systems are not only able to provide a way to maintain cell metabolic activities but also to deliver signals that guide cell activities. Offra *et al.* [7] observed guided cell behavior in 3D along microchannels. Currently, poly(dimethyl siloxane) (PDMS), also known as silicone, is the most commonly used material in micro-fabrication of fluidic channels [6, 8]. It is nontoxic, non-flammable, and can be used to culture cells. However, cells cannot be cultured within bulk PDMS materials. They can only be cultured on PDMS surface. Another material often used is poly(lactic-co-glycolic acid) (PLGA). It is a biodegradable, biocompatible synthetic biomaterial with several appealing advantages, including its adaptable chemistry and good mechanical properties; however, its performance in cellular interactions is not as good as expected due to acidic byproducts released during degradation. Compared to those synthetic biomaterials, natural biomaterials including collagen, alginate, chitosan, starch, and poly (hydroxybutyrate) gain more attention in tissue engineering due to their great biocompatibility, degradability, low cost of sourcing, and intrinsic cellular interactions [9]. In addition, hydrogels are popular for their high content of water, and they facilitate fast media transportation by means of diffusion and can be easily integrated to native extracellular matrix [10, 11]. Choi *et al.* [8] reviewed hydrogel-based micro-fluidic fabrication techniques thoroughly and discussed shortcomings. First of all, the ability to create intra-complex architectures in hydrogels needs to be greatly extended. Second, mechanical properties of hydrogels should be improved to sustain a 3D micro-fluidic network in tissue constructs having biologically and clinically relevant sizes. Current methods are limited to fabricating micro-fluidic hydrogels with either simple channel architecture or limited tissue thickness.

In this research, a new fabrication approach is presented through development of novel printable micro-fluidic channels in the form of hollow filaments. Micro-fluidic channels presented in this work not only enable transport of media to the cellular assembly, but can also support the mechanical integrity of the cellular environment in 3D. The printed micro-fluidic channels have greater flexibilities compared with previously discussed micro-fluidic channel fabrication methods. Complex 3D shapes can be achieved using a layer-by-layer bioadditive process through a computer-controlled system without the need for post-processing following fabrication. The proposed method generates micro-channels with an

average diffusion distance considerably smaller than the hydrogel diffusion limit (approximately 200 μm), which, theoretically, allows the printed micro-fluidic channels to provide sufficient oxygen transport.

In this work, a pressure-assisted freeform fabrication platform was developed with a coaxial nozzle dispenser unit to print hollow filaments. Sample structures were printed through the computer-controlled system. The dispending rheology and media flow characteristics through the coaxial nozzle system are studied, and the effects of biomaterial concentration, crosslinker concentration, and dispensing parameters are explored to understand bio-printability of micro-fluidic channels. To further evaluate our system, cell viability and functional analysis were performed. In addition, feasibility of oxygenized cell media perfusion is also demonstrated through printed microfluidic channels.

2. Materials and Methods

2.1 Coaxial nozzle Manufacturing

In this research, coaxial nozzles were fabricated using three fluid dispensing tips. This nozzle assembly consists of a feed tube, an outer tube, and an inner tube, as shown in figure 1(a). The feed tube is used to feed the hydrogel into the cavity formed between the outer and inner tubes while the cross-linker is fed through the inner tube to create the hollow filament, as shown in figure 1(a). A cross-sectional view of this nozzle is also demonstrated in figure 1(b). A hole with the same outer diameter as the feed tube was created in the barrel of the outer tube to attach the feed tube. The luer lock hub on the barrel of the outer tube was removed using a lathe, and the tip was ground to ensure that the inner and the outer dispensing tips were even. The feed tube was inserted until it was flush with the inner diameter of the barrel, sealed with J-B KWIK 4 minute epoxy, and reinforced with J-B STIK steel-reinforced epoxy putty. The two tubes were aligned concentrically using a stainless steel fixture manufactured using micro-milling. Then, the tubes were sealed with J-B KWIK 4-minute epoxy reinforced with J-B STIK steel-reinforced epoxy putty.

2.2 Experimental Setup

The experimental setup consists of a single-arm robotic printer (EFD® Nordson, East Providence, RI, USA) with a motion unit, a pressure regulator (EFD® Nordson, East Providence, RI, USA), and a syringe pump (New Era Pump System Inc., Farmingdale, NY) where biomaterials can be printed through a pressure-assisted computer-controlled system (see figure 1(d)). The coaxial nozzle assembly is mounted on the robot arm (highlighted in figure 1(c) to deposit micro-fluidic channels. Sodium alginate, which is a hydrogel-driven natural polymer and widely used in tissue engineering applications [12-14], is printed using the coaxial nozzle assembly to test the system. The sodium alginate solution is dispensed through the sheath section of the coaxial nozzle by compressed air, while the calcium chloride solution is dispensed through the core section of the coaxial nozzle (see figure 1(b)). When the two solutions contact, crosslinking (or gelation) starts, and a tubular gel is obtained with a hollow channel. Two coaxial nozzle assemblies are used in this paper: an assembly with 26 gauge (230 μm inner diameter (I.D.), 457 μm outer diameter (O.D.)) inner needle, and an 18 gauge (840 μm I.D., 1270 μm O.D.) outer needle used for the experiment

in Section 3.1, and another assembly with a 23 gauge (330 μm I.D., 650 μm O.D.) inner needle and an 18 gauge (840 μm I.D., 1270 μm O.D.) outer needle used for the experiment in Section 3.2. The coaxial nozzle used in Section 3.2 had a larger outer diameter of the inner nozzle that reduced the filament thickness. This allowed us to evaluate and understand the effect of dispensing parameters on functional microfluidic wall thickness further. Particularly, we tested whether microfluidic channels with thinner wall function as thicker ones. More than 50 pieces of data (10 different random segments from each of 5 printed microfluidic channels) were obtained for each group of experiments and subsequently analyzed using Minitab 14. Upon printing, both core and filament diameters of micro-fluidic channels were measured using a digital microscope (Motic®, BA310, Motic Incorporation Inc., Canada).

2.3 Materials

Sodium alginate (purchased from Sigma Aldrich, United Kingdom) and calcium chloride ($CaCl_2$) (purchased from Sigma Aldrich, Japan) was used to form the hydrogel. 3-6% (w/v) sodium alginate was dissolved in deionized water and placed in a shaker for 10 hours at 120 rpm at room temperature. Similarly, 2-5% (w/v) calcium chloride solutions were prepared using deionized water. Food dye (purchased from August Thomsen Corporation, USA) was used to differentiate the sheath section from the core section of hollow filaments for visualization purposes.

2.4 Cell Preparation

Bovine cartilage progenitor cells (CPCs) were cultured at 37 °C in 5% CO_2 in DMEM/F12 (1:1) supplemented with 10% fetal bovine serum (FBS), 50 μg/μl L-ascorbate, 100 μg/μl penicillin, 100 μg/ml streptomycin, and 2.5 μg/μl Fungi zone. Culture media was changed every other day. CPCs were passaged onto tissue culture dishes, and passage 3 cells were used for bioprinting. Cells were harvested by 0.25% Trypsin-EDTA (Life Technologies, NY) prior to printing. The alginate solution was prepared by adding UV-sterilized sodium alginate powder into DMEM-base culture media. Cells were mixed with the sodium alginate solution (2% w/v in DMEM-based media) immediately after harvesting and were kept at room temperature before printing.

2.5 Viability Analysis

For cell viability assay, CPCs were encapsulated in hollow filaments through the coaxial printing process, as described in Section 2.2, and underwent confocal imaging studies at day 1, day 4, and day 7. Hollow filaments were stained with calcein acetoxymethylester (calcein AM) and ethidiumhomodimer-2 (Invitrogen), at a concentration of 1.0 mM each. Calcein AM is metabolized in living cells to form a bright green fluorescent product that accumulates in the cytosol. Ethidium homodimer is a red fluorophore that stains the DNA of nonviable cells but cannot penetrate living cells with intact plasma membranes. The staining medium was aspirated, and new medium was added to wash off any residual stains on the hollow filament surface before fluorescent illumination. After a 30-minute incubation period, hollow filaments were imaged using an Olympus FluoViewTM FV1000 laser scanning confocal microscope (LSCM) (Olympus NDT Inc., MA). Z-axis projections were assembled from images of the hollow filaments from the surface to the bottom with a depth

of 1600 μm at 50 μm intervals. ImageJ (National Institutes of Health, Bethesda, MD) was used for automated counting of red- and green-stained CPCs in z-axis projections, and percentages of viable cells were calculated. The percentage of viable cells for each sample was calculated by averaging the values of three different projections, each composed of six planes.

2.6 Functional Analysis of CPCs

To evaluate cell function after the bioprinting process, CPC-encapsulated alginate hollow filaments were subjected to two weeks of culture in DMEM-based media. At the same time, CPCs also underwent monolayer culture as a control group. Encapsulated CPCs were then released from hollow filaments by dissolving them in dissolving buffer (55 mM sodium citrate, 30 mM EDTA, 0.15 M NaCl). Cells were centrifuged and washed twice in PBS (InvitrogenTM Life Technologies, Carlsbad, CA). Then the pellets were homogenized in TRIzol® reagent (InvitrogenTM Life Technologies, Carlsbad, CA), and total RNA was extracted using the RNeasy Mini Kit (Qiagen, Valencia, CA) according to the manufacturer's instructions. Cartilage-specific gene expression (collagen type II, aggrecan, and Sox9) was measured by real-time PCR in monolayer-cultured CPCs and alginate-encapsulated CPCs. Collagen type II is the basis for articular cartilage, and the collagen type II gene is a marker related to chondrocyte phenotype and function. Aggrecan, also known as cartilage-specific proteoglycan core protein (CSPCP), is a protein that is encoded by the ACAN gene in humans. The encoded protein is an integral part of the extracellular matrix in cartilage tissue. Sox-9 is a transcription factor related to chondrogenic differentiation, which is the main function of CPCs. PRG-4 is a gene encoded for proteoglycan 4 or lubricin, which is a protein that acts as an articular joint cell lubricant. The relative fold change in the qPCR study was the expression ratio derived from $2^{-\Delta\Delta Ct}$, where $\Delta\Delta C_t = \Delta Ct_{reference} - \Delta Ct_{target}$. Primers were purchased from Integrated DNA Technologies (Coralville, IA). Table 1 provides information about the primers used in real-time PCR analysis.

2.7 Statistical Analysis

The statistical significance of experimental data for the dimensional analysis of fabricated filaments was determined by one-way analysis of variance (ANOVA) with a significance level $p < 0.05$ in Minitab 16. The paired-wise test was combined with the Tukey post-hoc test at a significance level $p < 0.05$ and used for the cell functionality study in SPSS.

3. Results and Discussions

3.1 Effect of Material Concentration on Printed Filament Dimensions

Figure 2 shows a sample printed filament using 2% $CaCl_2$-4% alginate solutions. The average filament diameter was 445 μm. The thickness of the ungelled section was measured as 794 μm. This can be explained by the following phenomena. During the dispensing process, crosslinker was flowing through the core section of the filament, and diffusion was observed across the filament wall. Gelation of alginate occurred through the crosslinking mechanism, in which divalent cations ionically interacted with carboxylate anions of α-L-guluronic acid (G units) monomers, forming ionic bridges between different polymer chains

[18]. As long as divalent cations of Ca^{2+} ions contacted and exchanged with Na^{+} ions of G units of alginate, gelation started.

The main advantage of the gelation process is that it occurs gently under mild conditions and at room temperature without producing any toxic components [10]. Gelation depends on crosslinker and alginate concentrations as well as the flow rate of crosslinker through the core section. Due to low Ca^{2+} concentration in 2% $CaCl_2$ solution, only a small portion of the deposited alginate was cross-linked. This can be alleviated by increasing the concentration of $CaCl_2$.

In this section, the effects of alginate and its crosslinker ($CaCl_2$) concentration on printed filament dimensions are presented. Various combinations of alginate concentration and $CaCl_2$ were used. The results shown in figure 3(a) were obtained from an experiment conducted with 4% alginate cross-linked with different $CaCl_2$ concentrations. Alginate dispensing pressure and $CaCl_2$ dispensing rate were fixed at 6.6 ml/min and 4.15 ml/min, respectively. These parameters were selected because they resulted in functional microfluidic channels. The data showed a normal distribution with a p-value smaller than 0.05. Different crosslinker concentrations generated different filament dimensions due to a diffusion-dependent gelation process occurring throughout the cross-section of filaments. The results reveal that there is no distinct trend between crosslinker concentration and filament dimension. This can be explained by the diffusion phenomena, where the diffusion process is not only mediated by the change in concentration values, but also affected by ion size, hydrodynamic resistance, and crosslinking chemistry [15]. For 4% alginate concentration, the smallest filament diameter was obtained at 2% $CaCl_2$, where the smallest filament diameter was 617 μm with a filament wall thickness of 175 μm. The core-to-filament ratio (core diameter/filament diameter) was approximately 44%, which indicated that 19% less biomaterial volume was used compared to the same diameter cylindrical filament printed with traditional nozzle systems [16].

Similar experiments were conducted to understand the effect of sodium alginate concentration on printed filament dimensions, where $CaCl_2$ concentration was set to 4% (see figure 3(b)). The data showed a normal distribution with p-value smaller than 0.05. The smallest filament was obtained at 4% alginate cross-linked with 4% $CaCl_2$. The results revealed that there was no distinct trend between alginate concentration and filament dimensions. Indeed, the dimensions of printed filament were affected by the diffusion rate of Ca^{2+} ions, which was a function of alginate concentration and the thickness of alginate ejected from the coaxial nozzle. In other words, alginate concentration affected the diffusion rate of Ca^{2+} ions as well as the thickness of the hollow filament ejected from the nozzle per the fixed dispensing pressure.

3.2 Effect of Dispensing Rate on Filament Dimensions

In this section, the effect of dispensing rate on printed filament dimensions is presented. In this experiment, 4% alginate and 4% $CaCl_2$ were used while the smallest diameter of fully-crosslinked filament could be obtained using this combination as presented in Section 3.1. In general, we aimed to obtain fully-crosslinked filaments with the smallest diameter to enable effective media transport and fully gelled filaments without leaving any toxic components in

the cellular environment. Alginate dispensing pressure and $CaCl_2$ dispensing rate were varied to understand the effect of dispensing rates on filament dimensions. Data showed a normal distribution with p-value smaller than 0.05.

Figure 4(a) was obtained with the alginate dispensing rate fixed at 0.5 ml/min and the $CaCl_2$ dispensing rate levels set at 2, 3, and 4 ml/min. A smaller alginate dispending rate was applied compare to the one used in Section 3.1 due to the smaller opening in the coaxial nozzle used for this experiment. The results showed that both filament diameter and core diameter increased when $CaCl_2$ dispensing rate increased because of higher radial forces acting on the filament wall due to greater internal flow speed. Figure 4(b) showed the results of an experiment conducted with the $CaCl_2$ dispensing rate fixed at 2ml/min and the alginate dispensing rate set at 0.5, 1, and 1.2 ml/min. Similar results were obtained in this experiment. Filament diameter, core diameter, and filament thickness increased as alginate dispensing rate increased. This was due to the higher volume of alginate ejected per unit time resulting in greater filament diameter and thickness. Results in figure 4(c) concluded that core-to-filament ratio (core diameter/filament diameter) increased as the relative speed between $CaCl_2$ flow and alginate flow increased. This could be explained by increased diffusion rate through the alginate network in addition to higher radial forces exerted on the filament wall. Although smaller filament wall thickness (in other words, higher core-to-filament ratio) was desirable, a further increase in this ratio over 45% degenerated the mechanical integrity of filaments and caused non-uniform channels.

3.3 Fabrication

In this research, structural integrity was highly desired because printed micro-fluidic channels would later be used to transport media. Fabrication was performed with 4% alginate solution with a dispensing rate of 0.2 ml/min, which has demonstrated acceptable cell viability [17] and good structural integrity. 4% crosslinker solution was dispensed at 1.5ml/min for gelation purposes. The nozzle velocity was set at 14 mm/s. Figure 5(a) shows a sample printed filament fabricated using alginate mixed with green food dye for visualization purposes, where yellow food dye solution was transported through the hollow channel and showed non-blocked uniform filament geometry. Figure 5(b) illustrates the smallest printed sample under a digital microscope showing uniform wall thickness. The average inner and outer diameters of the fabricated hollow filaments were approximately 135 μm and 309 μm, respectively. Compared to the hydrogel diffusion limit of 200 μm presented in the literature [8], the printed micro-fluidic channels with 87 μm wall thickness are promising for efficient oxygenation and for nutrient and waste transportation. Figure 5(c) demonstrates a printed sample of a single-layer micro-fluidic channel network with arc turns to prevent channel blockage providing smooth transport of media. In addition, 8-layer micro-fluidic channels were printed to demonstrate the effectiveness of the fabrication platform (see figure 5(d)).

Although printing of sodium alginate has been demonstrated in the form of cylindrical filaments in the literature [3, 6-7], printing hollow filaments has its own challenges due to its complex geometry causing structural integrity issues during the fabrication process. Optimal dispensing parameters thus play a critical role in generating hollow filaments without

channel blockage. For instance, the relative speed of the coaxial nozzle (robot arm) and the dispensing speed determine the quality of the printed filaments. When the nozzle velocity (the velocity of the robot arm holding the coaxial nozzle) was considerably greater than the dispensing speed, then discontinuities and ruptures were observed during the printing process, dramatically preventing media transport. If the nozzle velocity, on the other hand, was considerably slower than the dispensing speed, then the filaments were printed with relatively greater wall thickness and non-uniformities were observed along the filament. This would eventually slow down the diffusion rate of media across the filament wall. We also performed a study to test the feasibility of media flow through printed complex patterns. Figure 6(a) illustrates oxygenized media perfusion through a printed cellular micro-fluidic channel approximately 44 cm in length and 1 mm in width with 500 μm lumen diameter. We perfused oxygenized cell media and circulated it through the channel without any blockage or swirling, which shows great potential for developing embedded channels serving as a vascular network for thick tissue fabrication. Direct printing of these channels allowed them to be integrated within a hybrid bioprinting platform and also facilitated patterning them into very complex shapes. We also embedded microfluidic channels within multi-layer hydrogel by printing them in between to demonstrate the feasibility of media flow under mechanical loading induced by the weight of the bulk hydrogel (see figure 6(c)). The media was successfully perfused through the channels.

3.4 Mechanical Properties of Printed Micro-fluidic Channels

While hollow filaments were fabricated to be used for providing fluid transport in future studies, we also analyzed mechanical integrity. Particularly, microfluidic channels were subjected to tensile stress during the media perfusion process (when the ends were connected and fixed to a perfusion chamber), and this could result in failures such as rupture of channels when the media flow rate was high. Figure 7 illustrates a multi-scale finite element analysis of hollow filaments under uniaxial tensile loading performed using the ANSYS 12 software package. Material properties of gels formed through crosslinking of various alginate and $CaCl_2$ concentrations, including Poisson's ratio ($\approx$0.31 [18]) and modulus of elasticity, were obtained from the literature [16] as presented in figures 7(e)-(f). In figure 7(a), meso-scale analysis is shown with a tensile uniaxial load applied from one side of the filament with the other side fixed. Per the applied load 0.7 Pa, a maximum 1.7 μm deformation was generated. In figure 7(b), a micro-scale finite element analysis was performed. The analysis revealed that the deformation on filaments increased from the core to the external boundary throughout the cross-sectional profile. The tendency of the core section with better structural integrity will thus provide better fluid transport capabilities for our future studies.

The effects of alginate and crosslinker concentrations on mechanical properties were demonstrated in figures 7(c)-(d). Figure 7(c) showed that there was an almost linear relationship between the displacement and the alginate concentration. As the alginate concentration increased, displacement decreased. There is also a similar relationship between the displacement and $CaCl_2$ concentration. Increasing crosslinker concentration resulted in reduction in the displacement amount. During analysis of hollow filaments, the

same length values were used, but cross-sectional geometry was set to be the mean value of the filament dimensions presented in figure 3.

3.5 Viability Analysis of Encapsulated CPCs

Cells were evenly distributed in alginate solution before printing and were successfully encapsulated into hollow filaments during the fabrication process. Confocal imaging revealed that few cells were dead (ethidium homodimer) and that most of the cells were stained with calcein AM (green) two days after cell encapsulation (see figure 8).

On day 4 and day 7, although a few cells were stained with ethidium homodimer (red), most of the cells were still viable. Image J analysis revealed that initial cell viability was around 97.6±1.16% 1 day post encapsulation within hollow filaments and maintained high cell viability on day 4 (95.8±1.23%) and day 7 (95.1±1.67%) (see figure 9).

A z-axis stack of confocal images with 50 μm intervals is shown in figure 10, demonstrating live/dead cells and their distribution in printed microfluidic channels. Figures 10(e)-(f) show the hollow feature of the printed microfluidic channel.

3.6 Functional Analysis of Encapsulated CPCs

Gene expression analysis revealed relatively higher expression of cartilage-specific marker genes in CPCs encapsulated in hollow fibers versus monolayer-cultured CPCs. In real-time PCR analysis, collagen type II (COL-2), Sox-9 showed an over two-fold change, which indicated that CPCs were better differentiated towards chondrogenic lineage, making cartilage-specific protein to serve as extracellular matrix.

Aggrecan genes (ACAN) were up-regulated to over 12-fold in bioprinted hollow filaments, which further supports that alginate hollow filament is an ideal environment for CPCs to differentiate and carry out their cartilage-producing function. More importantly, the lubricin gene PRG-4 also showed over a two-fold higher expression in hollow fibers (see figure 11). This observation demonstrated that CPCs cannot only differentiate towards chondrogenic lineage, but also can produce lubricant to fulfill normal joint function. In cell viability experiments, the maintained high cell viability demonstrates the biocompatibility of the proposed platform. The coaxial nozzle system does not only enable fabrication of micro-fluidic channels, but also allows encapsulating and printing cells with minimal cell damage. The higher expression of Col-2, ACAN, Sox-9, and PRG-4 genes in hollow filaments encapsulating CPCs further confirmed that the cells are not only viable, but also functional. Although we performed gene expression studies without any cell-type-specific growth factors or culture methods, significant results are obtained compared to those obtained from the monolayer culture. Considering the channel at the center of the filament, another advantage of hollow filaments is that proximity of encapsulated cells to the media on multiple sides further improves cell viability when compared to the cell viability in non-hollow filaments.

4. Conclusion

In this paper, a new process is presented for the biofabrication of printable continuous micro-fluidic channels, which shows great potential in perfusing media that can be used to fabricate thick tissues or living organs in the near future.

The proposed approach has several advantages. First of all, complex 3D microfluidic network architecture can be achieved with controllable dimensions and mechanical properties using a layer-by-layer bioadditive process through a computer-controlled system. No post-processing is needed following the fabrication. In addition, microfluidic channels in 3D can serve as a scaffold with up to 21% less biomaterial volume than is used in traditional scaffolding. Adverse effects caused by biomaterial degradation can thus be partially lessened. Compared to the traditional scaffolding approach, where tissue scaffolds mainly provide extracellular matrixes with mechanical support, the proposed approach provides mechanical support to cellular assembly and also enables controlled fluid transport to and from the cells. The proposed approach can be easily integrated with the cell-printing process in tandem, which is promising in terms of seeding co-culture cells and developing heterogeneous organ and tissue structures in the near future. Tissue spheroids [19] or cell-encapsulated micro-beads [20] can be easily printed between these channels concurrently by building hybrid systems as presented in our recent work [21]. The printed micro-fluidic channels have the potential to allow media transport, including nutrients, water, and oxygen, by perfusing them through hollow channels; the waste will be removed from the system in the same manner. Although we used CPCs to test the fabrication system and microfluidic channels for cell viability, the proposed bioprinter platform can be used to print living cells such as endothelial and smooth muscle cells loaded within hollow filaments to create tubular tissue scaffolds for vascular tissue engineering.

5. Future Work

As future work, we will analyze media flow through micro-fluidic channels in the form of continuous hollow filaments using micro-scale particle image velocimetry (micro-PIV) to demonstrate the fluid flow capability in detail. Fluid diffusion rate across the channel shell will be studied to predict the effects of hydrogel properties on the transport of media. Furthermore, spheroids containing CPCs will be printed between filaments, and media will be pumped through the channels to characterize cell viability for cartilage tissue fabrication. In another future study, we will print tissue spheroids encapsulating stem-cell-derived insulin-producing cells (iPCs) with micro-fluidic channels for pancreatic organ printing.

Acknowledgments

This research has been supported by National Institutes of Health (NIH) and the Institute for Clinical and Translational Science (ICTS) grant number ULIRR024979. The authors would like to thank the University of Iowa Office of the Provost for the equipment support in development of the bioprinting setup and Mr. Omer Elgaali for assisting with finite element analysis of hollow filaments. The authors also thank the Ignacio V. Ponseti Biochemistry and Cell Biology Laboratory for the cell source and confocal microscope images.

References

1. Lanza, R.; Langer, R.; Vacanti, J. Principles of Tissue Engineering. 3. Elsevier; 2007.

2. Melchels FPW, Domingos MAN, Klein TJ, Malda J, Bartolo PJ, Hutmacher DW. Additive manufacturing of tissues and organs. Progress in Polymer Science. 2012; 37:1079–1104.
3. Mondy WL, Cameron D, Timmermans JP, Clerk ND, Sasov A, Casteleyn C, Piegl L. 2009 Computer-aided design of microvasculature systems for use in vascular scaffold production. 2009; 1:035002.
4. Norotte C, Marga FS, Niklason LE, Forgacs G. Scaffold-free vascular tissue engineering using bioprinting. Biomaterials. 2009; 30:5910–7. [PubMed: 19664819]
5. Lee W, Lee V, Polio S, Keegan P, Lee JH, Fischer K, Park JK, Yoo SS. On-demand three-dimensional freeform fabrication of multi-layered hydrogel scaffold with fluidic channels. Biotechnology and Bioengineering. 2010; 105:1178–1186. [PubMed: 19953677]
6. Ling Y, Rubin J, Deng Y, Huang C, Demirci U, Karp JM, Khademhosseini A. A cell-laden microfluidic hydrogel. Lab Chip. 2007; 7:756–762. [PubMed: 17538718]
7. Offra SN, Livnat N, Ruthy Z, Shy S, Dror S. Laser Photoablation of Guidance Microchannels into Hydrogels Directs Cell Growth in Three Dimensions. Biophysical Journal. 2009; 96:4743–4752. [PubMed: 19486697]
8. Choi NW, Cabodi M, Held B, Gleghorn JP, Bonassar LJ, Stroock AD. Microfluidic scaffolds for tissue engineering. Nat Mater. 2007; 6:908–915. [PubMed: 17906630]
9. Khalil S, Sun W. Biopolymer deposition for freeform fabrication of hydrogel tissue constructs. Material Science and Engineering: C. 2007; 27:469–478.
10. Drury JL, Mooney DJ. Hydrogels for tissue engineering: scaffold design variables and applications. Biomaterials. 2003; 24:4337–4351. [PubMed: 12922147]
11. Nelson CM, Tien J. Microstructured extracellular matrices in tissue engineering and development. Current Opinion in Biotechnology. 2006; 17:518–523. [PubMed: 16971111]
12. Ozbolat IT, Koc B. Modeling of Spatially Controlled Bio-molecules in Three-dimensional Porous Alginate Structures. Journal of Medical Devices. 2010; 4:041003.
13. Lin N, Lin J, Bo L, Weidong P, Chen S, Xu R. Differentiation of bone marrow-derived mesenchymal stem cells into hepatocyte-like cells in an alginate scaffold. Cell Proliferation. 2010; 43:427–434. [PubMed: 20887549]
14. Wang CC, Yang KC, Lin KH, Liu FH. A highly organized three-dimensional alginate scaffold for cartilage tissue engineering prepared by microfluidic technology. Biomaterials. 2011; 32:7118–7126. [PubMed: 21724248]
15. Ozbolat IT, Koc B. 3D hybrid wound devices for spatiotemporally controlled release kinetics. Computer Methods and Programs in Biomedicine. 2012; 108:922–31. [PubMed: 22672934]
16. Khalil, S. PhD Dissertation. Drexel University; Philadelphia, PA: 2005. Deposition and Structural formation of 3D Alginate Tissue Scaffolds.
17. Kong HJ, Smith MK, Mooney DJ. Designing alginate hydrogels to maintain viability of immobilized cells. Biomaterials. 2003; 24:4023–4029. [PubMed: 12834597]
18. Nguyen VB, Wang CX, Thomas CR, Zhang Z. Mechanical properties of single alginate microspheres determined by microcompression and finite element modelling. Chemical Engineering Science. 2009; 64:821–829.
19. Mironov V, Visconti R, Kasyanov V, Forgacs G, Drake CJ, Markwald RR. Organ printing: Tissue spheroids as building blocks. Biomaterials. 2009; 30:2164–2174. [PubMed: 19176247]
20. Xu C, Chai W, Huang Y, Marwald R. Scaffold-free inkjet printing of three-dimensional zigzag cellular tubes. Biotechnology and Bioengineering. 2012; 209:3152–3160. [PubMed: 22767299]
21. Chen H, Ozbolat IT. Manufacturing living things. Industrial Engineer. 2013; 45:30–34.

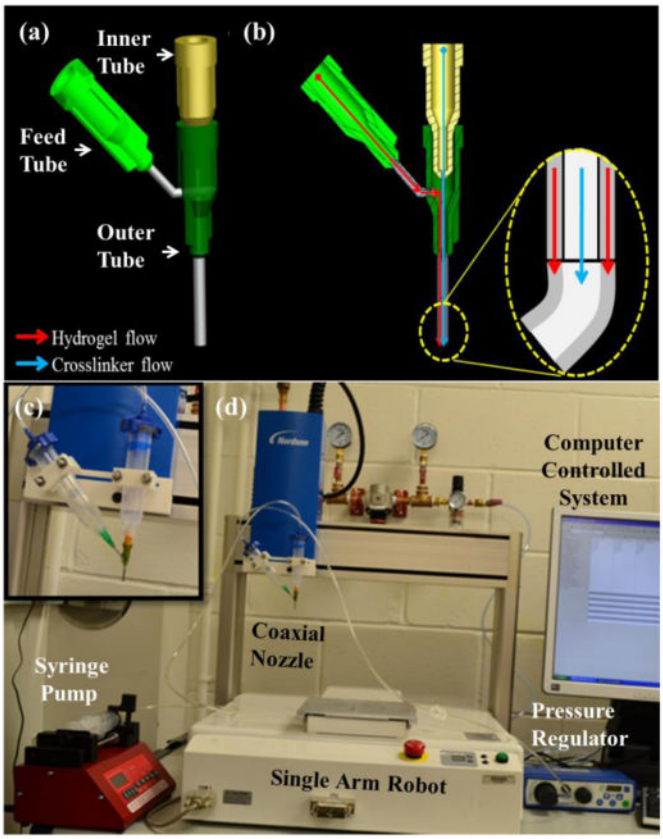

Figure 1.

The experimental setup: (a) 3D model of the coaxial nozzle, (b) cross-sectional view of coaxial nozzle assembly model with fluid flow paths for hydrogel and crosslinker solutions, (c) the coaxial nozzle system, and (d) the robotic printer platform.

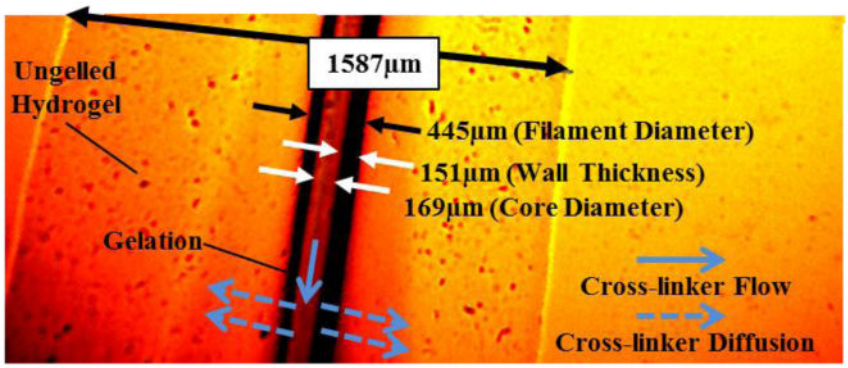

Figure 2.
Effect of hydrogel properties on gelation of hollow filaments.

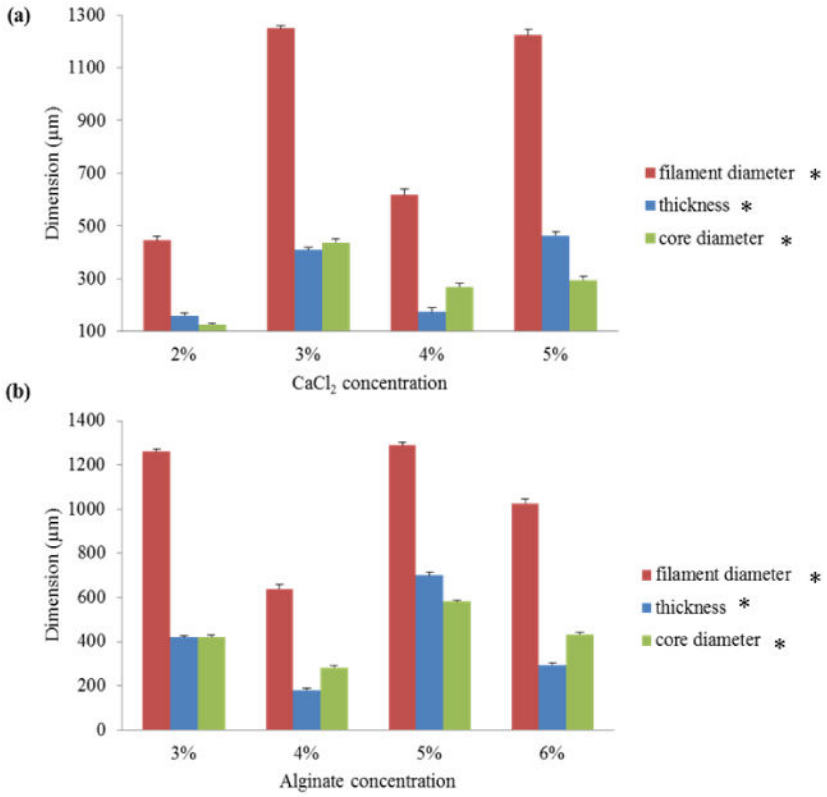

Figure 3. (a) Effect of $CaCl_2$ and (b) alginate concentration on hollow filament dimensions. (Single asterisk (*) indicates significant differences between groups ($p<0.05$))

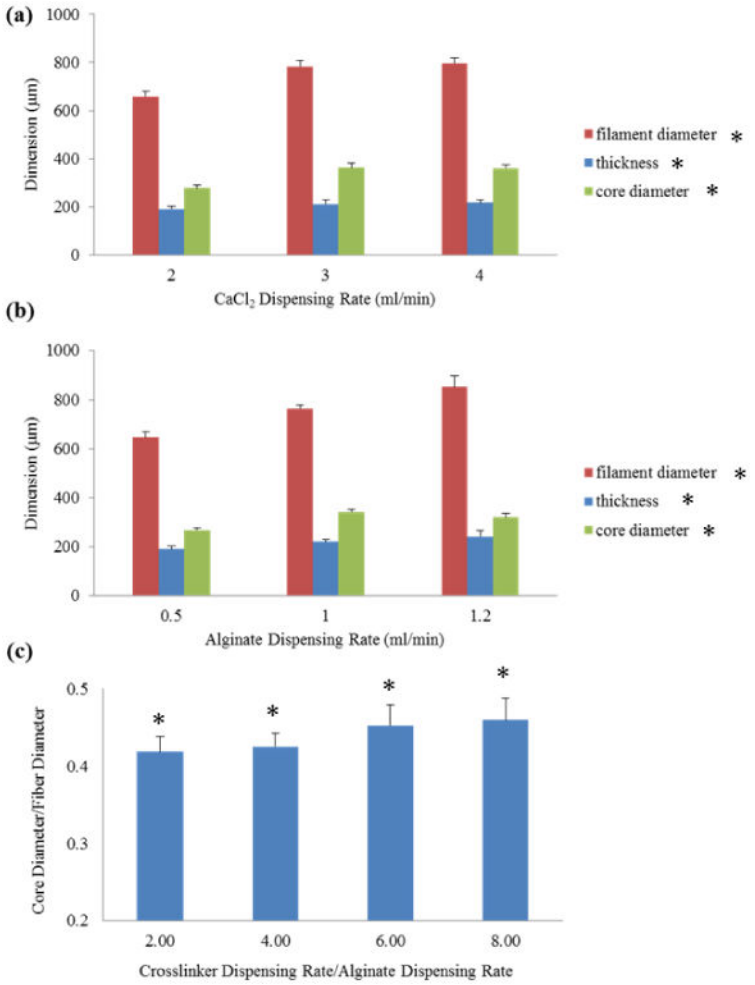

Figure 4. Hollow filament dimensions with different (a) $CaCl_2$ dispensing rates and (b) alginate dispensing rates, and core-to-filament ratio with different relative speed between crosslinker and alginate flow. (Single asterisk (*) indicates significant differences between groups ($p<0.05$))

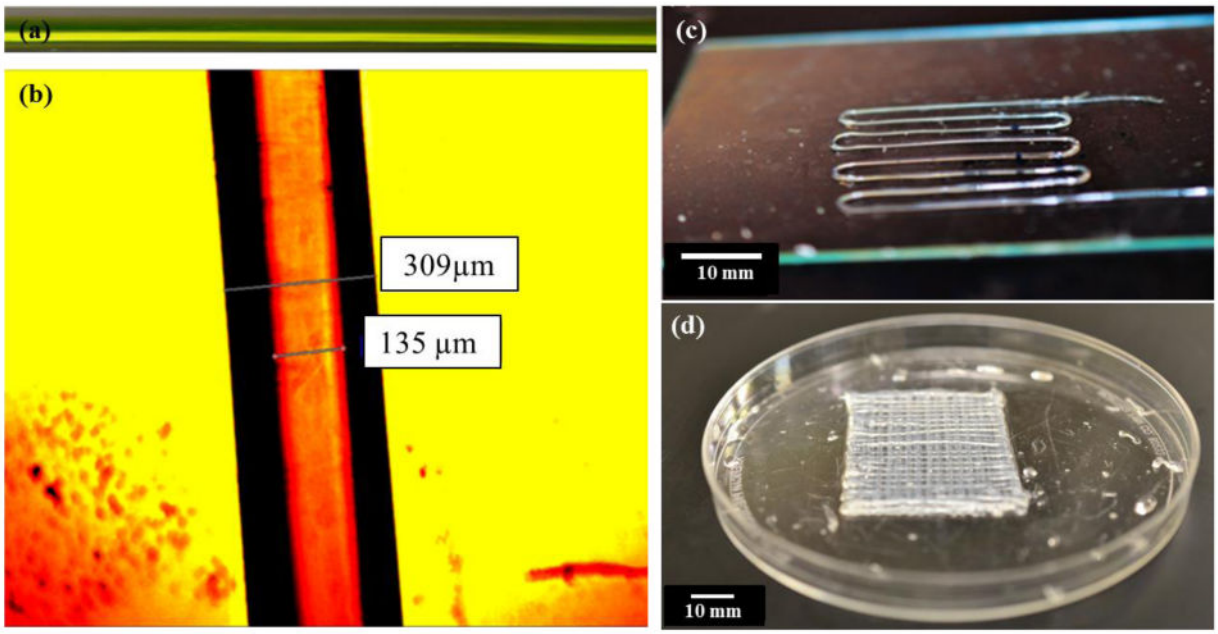

Figure 5.

Sample printed structures: (a) a printed filament allowing media transport shown with a yellow food dye, (b) an image of a single filament analyzed under a digital microscope, (c) a printed single-layer micro-fluidic channel, and (d) a printed 8-layer micro-fluidic channels.

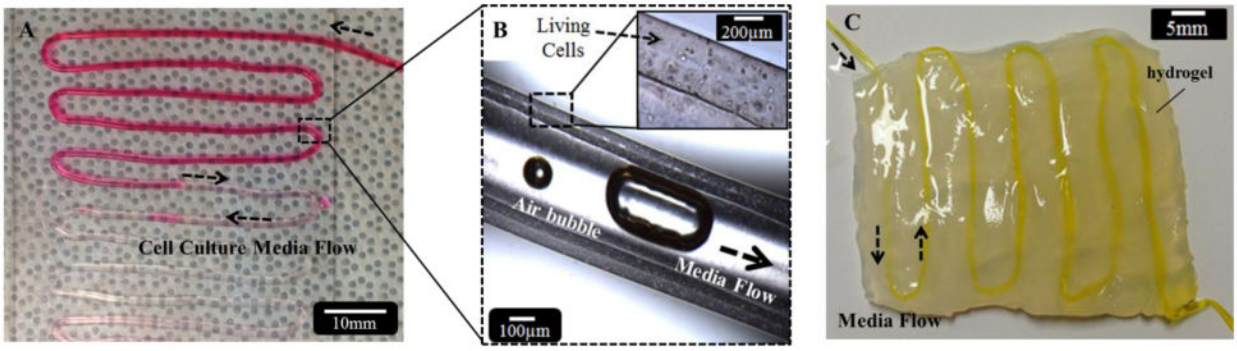

Figure 6.

(a) Perfusion of oxygenized cell type media, (b) media flow with intentionally generated air bubbles showing flow, and (c) embedding microfluidic channels within multilayer bulk hydrogel.

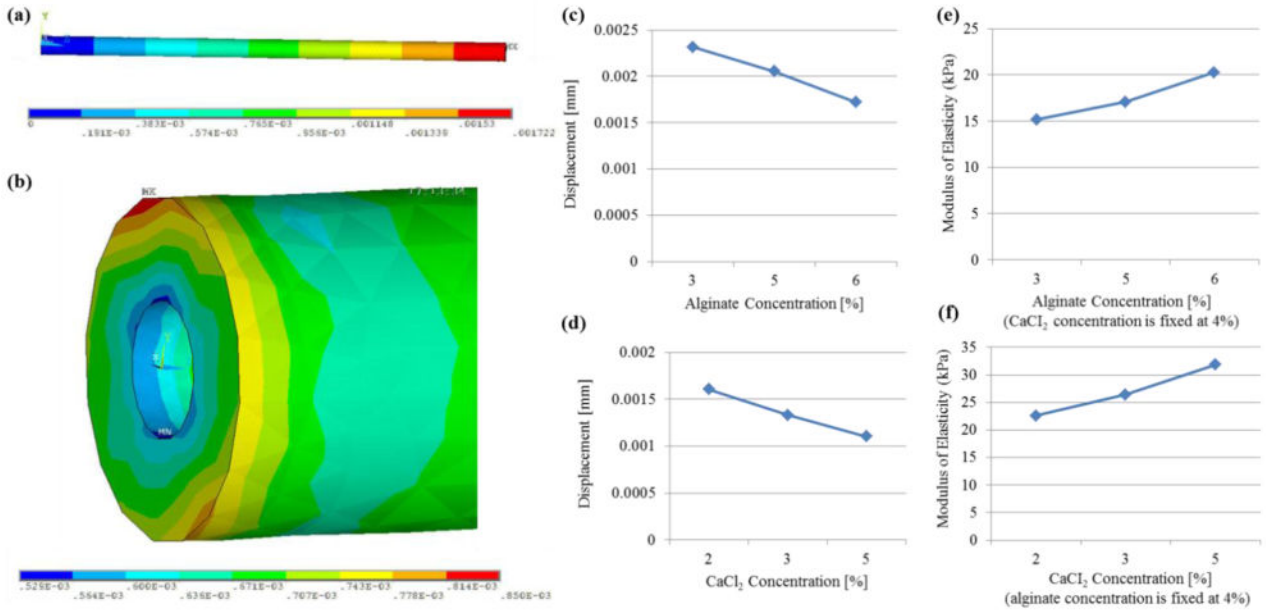

Figure 7.

Multi-scale uniaxial tensile testing of hollow filaments: (a) meso-scale analysis illustrating overall deformation on a 2 cm long filament and (b) micro-scale analysis along the cross-section, and the effect of (c) alginate and (d) crosslinker concentrations on tensile deformation of printed micro-fluidic channels and (e)-(f) corresponding modulus of elasticity values obtained from the literature [16].

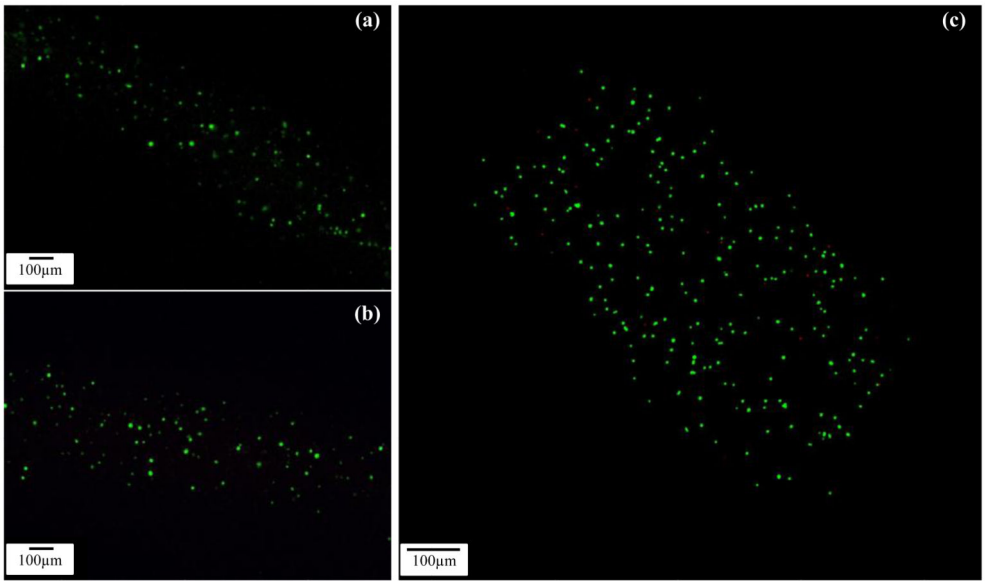

Figure 8.

Laser confocal imaging of viability staining. CPCs labeled with calcein AM and ethidium homodimer after cell encapsulation in an alginate hollow filament (cell viability assay) and imaged with confocal laser scanning microscope. Live and dead cells were fluorescent green and fluorescent red, respectively. (a-b) No dead cells were visible in Day 1 and Day 4 images and (c) a few dead cells were observed in the Day 7 image

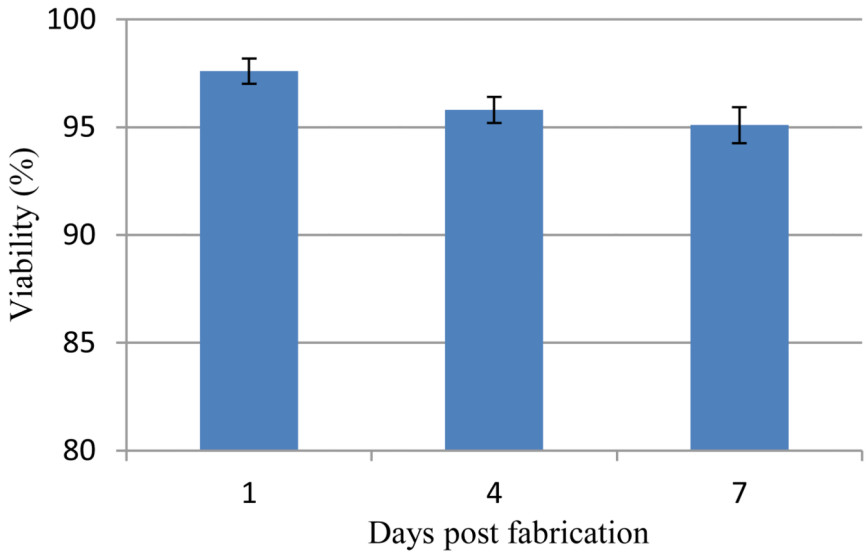

Figure 9.

Time course of CPC viability after the bioprinting process. Cell viability was analyzed using Image J. Each symbol represents the average of the results for three z-projections composed of six planes from confocal laser imaging. The error bars indicate standard deviations (n=3).

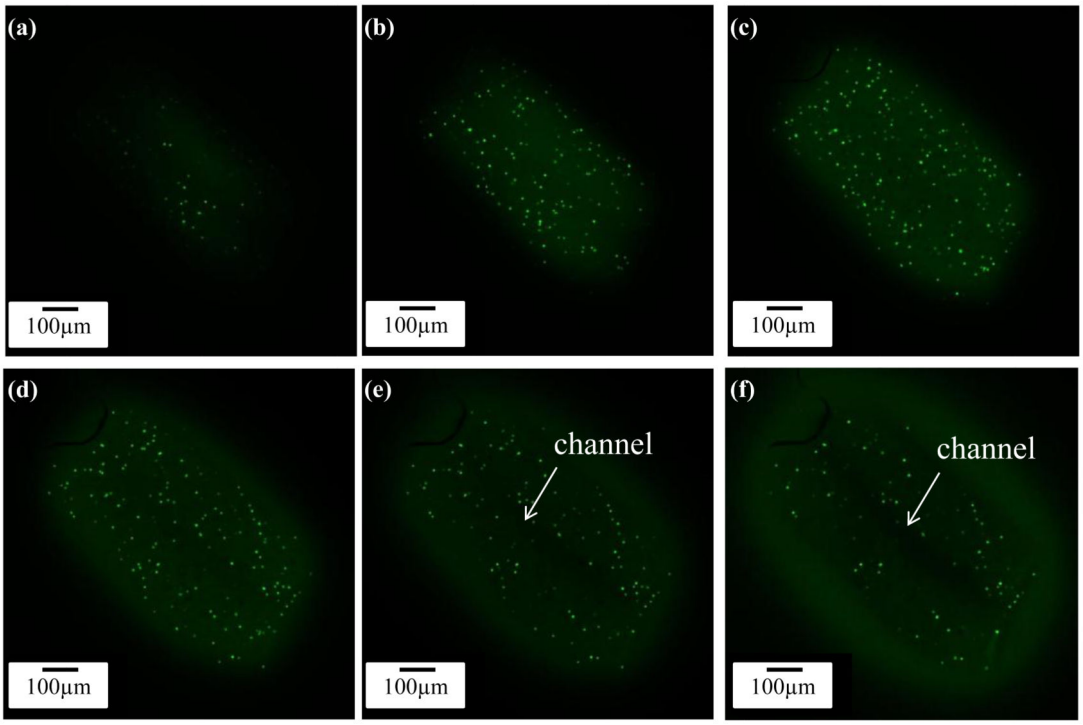

Figure 10.

Confocal images showing hollow property of filaments: (a-f) z-projection from top to center of a cell-encapsulated hollow filament, with 50 μm intervals showing the solid wall of fabricated filaments and the hollow channel in the center.

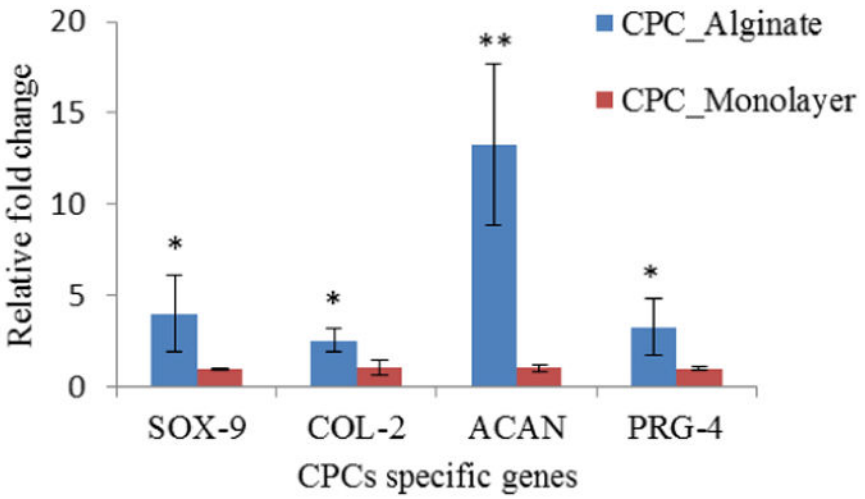

Figure 11.

Real-time PCR showed relatively higher expression of cartilage-specific marker PRG-4, Sox-9, COL-2: all showed over two-fold up-regulation in alginate hollow filament encapsulating CPCs after bioprinting, compared with CPCs in monolayer culture. ACAN showed over 12-fold higher expression level. The error bars indicate standard deviations (n=3). (Single asterisk (*) and double asterisks (**) represent significant differences, $P<0.05$ and $P<0.01$, from the monolayer control group, respectively.)

Table 1

Primer information for real-time PCR

Primer	Forward	Reverse
B-actin	TCGACACCGCAACCAGTTCGC	CATGCCGGAGCCGTTGTCGA
Collagen type II	AAGACGCAGAGCGCTGCTGG	GGGTCTCTACCGCGCCCTCA
Aggrecan	ACCAGACAGTCAGATACC	GCAGTAGACATCGTAGG
Sox-9	CGGTGGTGTTTGGCCATGTAATGA	GAGAGAGGGGAGTCCTATCCTGGT